NEOPLASIA
www.neoplasia.com

Volume 21 Number 9 September 2019 pp. 932–944 932

# Dual CTLA-4 and PD-L1 Blockade Inhibits Tumor Growth and Liver Metastasis in a Highly Aggressive Orthotopic Mouse Model of Colon Cancer[1,2]

**E Fiegle*, D Doleschel*,†, S Koletnik*, A Rix*, R Weiskirchen†, E Borkham-Kamphorst†, F Kiessling* and W Lederle*,***

*Institute for Experimental Molecular Imaging, Medical Faculty, RWTH Aachen University, Germany; †Institute of Molecular Pathobiochemistry, Experimental Gene Therapy and Clinical Chemistry (IFMPEGKC), RWTH Aachen University Hospital, Germany

## Abstract

Immune checkpoint inhibitors have shown clinical benefit in several cancer entities including metastatic microsatellite instable colorectal carcinomas. However, for the majority of metastatic colorectal carcinomas the potential and limitations of immune checkpoint inhibition is not fully understood. In this study, the effects of sole and dual CTLA-4 and PD-L1 blockade were investigated in a microsatellite stable highly aggressive orthotopic mouse model of colon cancer. Dual CTLA-4 and PD-L1 inhibition resulted in tumor growth stagnation and completely blocked liver metastasis. Sole CTLA-4 and PD-L1 inhibition only moderately reduced metastatic spread of the colon cancer cells, though CTLA-4 blockade being superior to PD-L1 inhibition. Dual immune checkpoint blockade and sole CTLA-4 inhibition significantly increased intratumoral CD8+ and CD4+ T cells and reduced FOXP3+/CD4+ Treg cells. This was associated with increased expression levels of the pro-inflammatory Th1/M1-related cytokines IFN-γ, IL-1α, IL-2, and IL-12. Moreover, tumors treated with combined immune checkpoint blockade showed the strongest increase in intratumoral iNOS+ macrophages, reduction of PD-L1+ and Tie2+ macrophages and the lowest expression of M2/Th2-related IL-4, TARC and COX-2. The assessment of further microenvironmental changes by DCE-MRI and immunohistology revealed no alterations in functional tumor vascularization upon combined immune checkpoint blockade, but a significant increase in intratumoral fibroblasts and collagen I deposition. Thus, the synergistic inhibitory effects of dual immune checkpoint inhibition can be explained by anti-tumorigenic T cell responses mediated by CTLA-4 inhibition and M1 macrophage polarization predominantly induced by PD-L1 blockade. This was accompanied by pronounced fibroblast activation highlighting the interconnection between immunogenicity and desmoplasia.

*Neoplasia (2019) 21, 932–944*

Abbreviations: ARG1, arginase-1; COX-2, cyclooxygenase-2; CRC, colorectal cancer; CTLA-4, cytotoxic T-lymphocyte-associated protein 4; DCE-MRI, dynamic contrast enhanced MRI; FAP, fibroblast-activated protein; FOXP3, forkhead box protein P3; iNOS, inducible nitric oxide synthase; IFN-γ, interferon- γ; MRC1, macrophage mannose receptor 1; PD-1, programmed death 1; PD-L1, programmed death-ligand 1; PDGF-B, platelet-derived growth factor B; PDGFR-β, platelet-derived growth factor receptor β; p.i., post-injection; s.c., subcutaneous; TARC, thymus and activation regulated chemokine; TEM, Tie2+ macrophages; TGF-β, transforming growth factor-β; TIE2, tyrosine kinase with immunoglobulin-like and EGF-like domains 2; Treg cells, regulatory T cells; VEGF-A, vascular endothelial growth factor A; VEGFR2, vascular endothelial growth factor receptor 2

Address all correspondence to: Dr. Wiltrud Lederle, PhD, Institute for Experimental Molecular Imaging, RWTH-Aachen University, Forckenbeckstrasse 55, 52074 Aachen, Germany. E-mail: wlederle@ukaachen.de

[1] Acknowledgements: Funding: This work was supported by the Interdisciplinary Centre for Clinical Research within the faculty of Medicine at the RWTH Aachen University [grant numbers No O3-9 and O3-1] and by the Deutsche Forschungsgemeinschaft (DFG) in the framework of the Research Training Group 2375 "Tumor-targeted Drug Delivery" grant 331065168. We acknowledge Gremse-IT GmbH for providing the software Imalytics Preclinical 2.0.

[2] Disclosure and conflict of interest: The authors declare no conflicts of interest.

Received 22 February 2019; Accepted 17 July 2019



1476-5586
https://doi.org/10.1016/j.neo.2019.07.006

## Introduction

Colorectal cancer (CRC) is the third most common type of cancer [1] counting more than 1.3 million new cases per year worldwide. 40–50% of patients with colorectal cancer die from distant metastases [2]. In the last two decades median overall survival of patients with metastatic CRC (mCRC) has increased from 18 up to 30 months [2,3]. This was mainly due to improved chemotherapy, the implementation of targeted therapies (VEGF and EGFR inhibitors [4]) and improvements in surgical management (resection of liver metastases) [2]. Nevertheless colorectal cancer remains the third-most common cause of cancer-related deaths [1] and metastatic stage of colorectal cancer still decreases the overall 5-year survival rate to 10% [2]. New therapeutic strategies and combinations of drugs are sorely needed to further improve overall survival of patients with metastatic colorectal cancer.

Immune checkpoint inhibitors have shown considerable clinical benefit in several cancer entities and are approved for some late-stage and metastatic cancers, e.g. melanoma, non-small cell lung cancer and bladder cancer [4,5]. Checkpoint inhibitors modulate the immune response and enhance endogenous anti-tumor activity by blocking receptors on T cells or other cells that inhibit T-cell activity [6]. T-cell activation is initiated through antigen recognition by the T-cell receptor. The amplitude of T-cell activation is regulated by co-stimulatory and inhibitory signals (the so called immune checkpoints). The balance between co-stimulatory and inhibitory signals is crucial for effective immunity, peripheral immune tolerance and preventing autoimmunity [7]. Different immune checkpoint inhibitors are used in (pre)-clinical research and treatment.

Cytotoxic T-lymphocyte associated antigen 4 (CTLA-4) is expressed on T cells to regulate T-cell activation by transmitting inhibitory signals to T cells. CTLA-4 binds to CD80 (B7–1) and CD86 (B7–2) on antigen-presenting cells and counteracts the effects of the co-stimulatory protein CD28. CTLA-4 predominantly down-regulates T-cell activation and response [8]. CTLA-4 blockade was shown to inhibit tumor progression by up-regulating effector T-cell activity and suppressing regulatory T cells (Treg cells) [6,9].

Programmed death-ligand 1 (PD-L1, B7-H1, CD274) binds to programmed cell death protein 1 (PD-1) or CD80. The major role of the PD-1/PD-L1 pathway is to limit the activity of T cells in peripheral tissues during the inflammatory response to infection and to restrain autoimmunity. PD-L1 is expressed on T cells, antigen presenting cells (dendritic cells and macrophages) and tumor cells and is up-regulated upon activation [10].

Promising results have been obtained for anti-PD-1 therapy in microsatellite instable/ mismatch-repair-deficient mCRC. A phase II study evaluating PD-1 blockade in tumors with mismatch-repair deficiency reported an immune-related progression-free survival rate of 78% for mismatch-repair-deficient CRC and 11% for mismatch-repair-proficient CRC, respectively [11,12]. The PD-1 inhibitor Pembrolizumab was approved by the US Food and Drug Administration in 2017 for treatment of metastatic solid tumors that are microsatellite instable or mismatch-repair-deficient, including CRC [13]. However, for therapy of microsatellite stable metastatic colorectal cancer, alternative approaches are required.

In pre-clinical research using subcutaneous (s.c.) colon cancer models, dual checkpoint blockade or the combination of a checkpoint inhibitor with other immune-modulatory therapies (e.g. vaccination strategies or anti-IL-6 or anti-IL-21 antibodies) significantly increased the anti-tumorigenic response [14–16]. However, the use of s.c. colon cancer models is disadvantageous for evaluating immune therapy as the immune microenvironment significantly differs between subcutaneous and gastrointestinal tissue [17]. Moreover, the effects of therapeutic agents on metastasis cannot be evaluated in subcutaneous tumors, because they hardly metastasize at all. We have previously established an orthotopic xenograft model of murine colon cancer, which metastasizes to the liver to investigate the effects of anti-tumorigenic agents in a clinically more relevant setting [18]. We have transferred this highly aggressive orthotopic model to syngeneic mice and investigated the effects of the immune checkpoint inhibitors anti-CTLA-4 and anti-PD-L1, which have different mechanisms of action on the immune cells. The effects of the immune checkpoint inhibitors on tumor progression and metastasis were analyzed as monotherapies, respectively, as well as in combination therapy. Longitudinal in vivo MR-measurements of tumor growth and vascularization were complemented by ex vivo analyses to explore the microenvironmental changes.

## Material and Methods

### *CT26 Cell Line*

CT26 murine colon carcinoma cells were cultivated in Dulbecco's Modified Eagle's Medium (DMEM, Gibco) supplemented with 10% FBS (Gibco) and 1% penicillin/streptomycin (Gibco) at 37 °C and 5% $CO_2$. The CT26 cell line was originally generated by exposing BALB/c mice to N-nitroso-N-methylurethane (NNMU) and is consequently syngeneic in BALB/c mice [19]. The cells were tested negative for mycoplasma by Hoechst stain and PCR.

### *Orthotopic Murine Colon Cancer Model (CT26)*

All animal studies were approved by the Governmental Review Committee on Animal Care. Six- to eight-week-old female BALB/c mice were purchased from Janvier. A two-step process was undertaken to induce orthotopic syngeneic colon tumors as described previously [18,20]. In the first step $1 \times 10^6$ CT26 tumor cells were inoculated subcutaneously into the right flank of mice. At a tumor size of approximately 500 $mm^3$, donor mice were sacrificed. The tumors were harvested, cut into 1–2 $mm^3$ fragments and stored in ice-cold PBS. Necrotic areas were discarded. In a second step, tumor pieces were implanted orthotopically as described by Hoffman et al. and Abou-Elkacem et al. [18,20]. For analgesia, carprofen (5 mg/kg body weight) was administered to the mice subcutaneously before surgery and every 12 hours after surgery for a total duration of 4 days. For surgical orthotopic implantation, mice were anesthetized with isoflurane (1.5%). The abdomen was shaved and disinfected. Subsequently a 5 mm laparotomy was conducted. The caecum was exposed and a tumor fragment was implanted below the serosa. The caecum was returned in the abdomen and peritoneum and skin were closed by suture. Wound-healing was supported with povidone-iodine cream (B. Braun Melsungen AG) and wound-healing spray (Beiersdorf AG Hansaplast). Mice that underwent surgery were able to recover for 4 days before initiation of the therapies and measurements.

### *Study Design and Therapies*

In total, 25 mice with orthotopic colon tumors were included for analysis of the treatment effects (Supplementary Figure S1). On day 4 after tumor implantation, mice were randomly divided into 4

experimental groups comprising at least 6 animals each and treatment was initiated. In the control group, mice received intraperitoneal (i.p.) injections of isotype control IgG antibodies (10 mg/kg body weight of polyclonal Syrian hamster IgG, BioXCell, and 10 mg/kg of rat IgG2b, BioXCell). The second and third group were treated i.p. with anti-mouse-CTLA-4 (10 mg/kg body weight, BioXCell, Clone:9H10) or anti-PD-L1 antibodies (10 mg/kg body weight, BioXCell, Clone: 10F.9G2, rat IgG2b), respectively. The fourth group received a combination of anti-CTLA-4 and anti-PD-L1 antibodies (both 10 mg/kg bodyweight, i.p.). Antibodies were applied on day 4, 7, 10 and 13 post-tumor implantation (p.i.). To determine tumor volume and vascularization, $T_1$/$T_2$-weighted and DCE-MRI imaging was performed on day 4, 7, 11 and 14 with a preclinical 1 T MR scanner (Bruker ICON). On day 14 all mice were euthanized. Orthotopic tumors and livers were resected and cryoconserved for immunohistochemistry. Livers were surveyed macroscopically for metastases.

### *MR Measurements*

For MR measurements mice were anesthetized with isoflurane (1.5%). A closed water heating system was implemented in the mouse bed in order to keep the temperature constant at 37 °C. The eyes of the mice were protected with eye ointment (Bepanthen, Bayer). Tumors were localized by transversal $T_1$-RARE sequences (repetition time, TR = 579.021 ms; echo time TE = 12 ms; echo spacing = 12 ms; rare factor = 2; flip angle = 90°; number of signal averages NSA = 8; field of view, FOV = 35 mm × 35 mm, matrix size = 256 × 256; slice thickness = 1.25 mm; voxel size = 0.137 mm × 0.137 mm × 1.25 mm, time = 7 min 24 s 688 ms). Tumor volume was measured using a $T_2$- RARE sequence (TR = 1681.175 ms; TE = 84 ms; rare factor = 8; excitation angle = 90°, refocusing angle = 180°; NSA = 8; FOV = 35 mm × 35 mm; matrix size: 192 × 192; slice thickness = 1.25 mm; voxel size = 0.182 mm × 0.182 mm × 1.25 mm; time = 5 min 22 s 785 ms). Tumor vascularization was assessed by dynamic contrast enhanced (DCE)-MR-measurements. In total, 80 sequential images were acquired per slice with a temporal resolution of 7.9 seconds, resulting in a total scan time of 10.53 min. After baseline measurements for approximately 2 minutes, 80 µl of the MR contrast agent Gadomer 17 (in vivo Contrast, Berlin) was injected slowly into a tail vein and a $T_1$-Flash sequence (T1w saturation recovery gradient echo) was accomplished (TR = 118 ms, TE = 6 ms; NSA = 1, repetitions = 80; matrix size = 64 × 64; field of view = 30 mm × 30 mm; flip angle 30°; slice thickness = 1.25 mm, voxel size = 1 mm × 1 mm × 1 mm). Tumor volume was quantified by encircling the tumor lesions in the $T_2$-weighted images in each slice using Imalytics preclinical 2.0 (Gremse-IT GmbH, Aachen) [21].

Tracer kinetic modeling was performed as described by Abou-Elkacem et al. [18,22]. The average signal per region was computed and the resulting signal-to-time curves were analyzed using the pharmacokinetic two compartment model of Brix and colleagues [23,24]. The provided parameter amplitude A relates to the relative distribution volume of blood in the tumor. Phantom experiments were performed in advance to prove the linearity between applied contrast agent concentration and signal intensity.

### *Immunofluorescent Stainings*

Immunofluorescent stainings were performed on 8 µm thick frozen slices of the tumors as described [18,25]. Methanol and acetone were used to fix the tissue in all cases except for CD4/FOXP3 staining. CD4/FOXP3 staining was performed on formaldehyde-fixed tissue, which was permeabilized before the application of the antibodies. Primary and secondary antibodies are provided in the Supplementary Methods. Images were obtained at an epi-fluorescence microscope (Axio Imager.M2, Zeiss) equipped with a high-resolution camera (AxioCam MRm Rev.3, Zeiss) and the AxioVision SE64 Rel.4.9 software (Zeiss). Quantification was performed as described in the supplements using ImageJ 1.50i software (National Institutes of Health).

### *Analysis of Cytokine mRNA Expression in Tumors*

Sections (à 50 µm) from each tumor were collected and RNA was extracted using the guanidine thiocyanate/CsCl method and the Purelink RNA Mini kit system (Invitrogen, Life Technologies) as described [26]. Total RNA concentration was determined with the NanoDrop 2000 spectrophotometer (Thermo Fisher Scientific), and 2 µg RNA per tumor sample were applied for cDNA synthesis using Superscript II reverse transcriptase and random hexamer primers (both from Invitrogen), resulting in a total volume of 200 µl. For individual quantitative real-time (q)PCR, 5 µl of cDNA was amplified in a total volume of 25 µl using the SYBR Green™qPCR SuperMix (Applied Biosystems, Life Technologies) and the Thermocycler CFX 96 touch (Bio-Rad). Relative levels of target mRNAs were calculated using the comparative CT method [27] and normalized to the expression of glyceraldehyde 3-phosphate dehydrogenase (GAPDH). The primers are listed in "Supplementary Methods".

### *Analysis of Cytokine Expression in Tumors*

The analysis of cytokine expression in tumors of the treatment groups at the protein level was done using different ELISA kits. Mouse Th1/Th2 Uncoated ELISA (Invitrogen) was used to determine the protein levels of IFN-γ, IL-2 and IL-4. IL-1α, IL-12, TGF-β, PDGF-BB, VEGF and COX-2 were measured with the Mouse IL-1 alpha/IL-1F1 DuoSet ELISA, Mouse IL-12 p70 DuoSet ELISA, Mouse TGF-β1 DuoSet ELISA, Mouse/Rat PDGF-BB DuoSet ELISA, Mouse VEGF DuoSet ELISA and Human/Mouse Total COX-2 DuoSet IC ELISA, respectively (all from R&D Systems). TARC was determined with the Mouse CCL17/TARC Quantikine ELISA Kit (R&D Systems). For protein extraction, various sections (of 50 µm thickness) from each tumor were collected and protein lysates were prepared using RIPA buffer (20 mM Tris–HCl (pH 7.2), 150 mM NaCl, 2% (w/v) NP-40, 0.1% (w/v) SDS, 0.5% (w/v) sodium deoxycholate) and cOmplete™ Protease Inhibitor Cocktail (Sigma-Aldrich) [28]. The total protein concentration of each tumor sample was determined using the DC protein assay (Bio-Rad Laboratories GmbH). Equal amounts of total protein (50 µg) were diluted with ELISA-Buffer (ELISA/ELISPOT Diluent, Invitrogen), or Reagent Diluent Concentrate 2 (R&D Systems), respectively. Cytokine amounts were determined according to the manufacturers' instructions.

### *Statistical Analysis*

Statistical analyses were performed using the software GraphPad Prism 5.01 (GraphPad Software). Data were analyzed statistically using one-way ANOVA and Bonferroni multiple comparison post hoc test (comparing the treatment groups to the control group) and are presented as mean ± standard deviation. Statistical significance $P < .05$, $P < .01$, $P < .001$ is presented as *, **, or *** respectively.

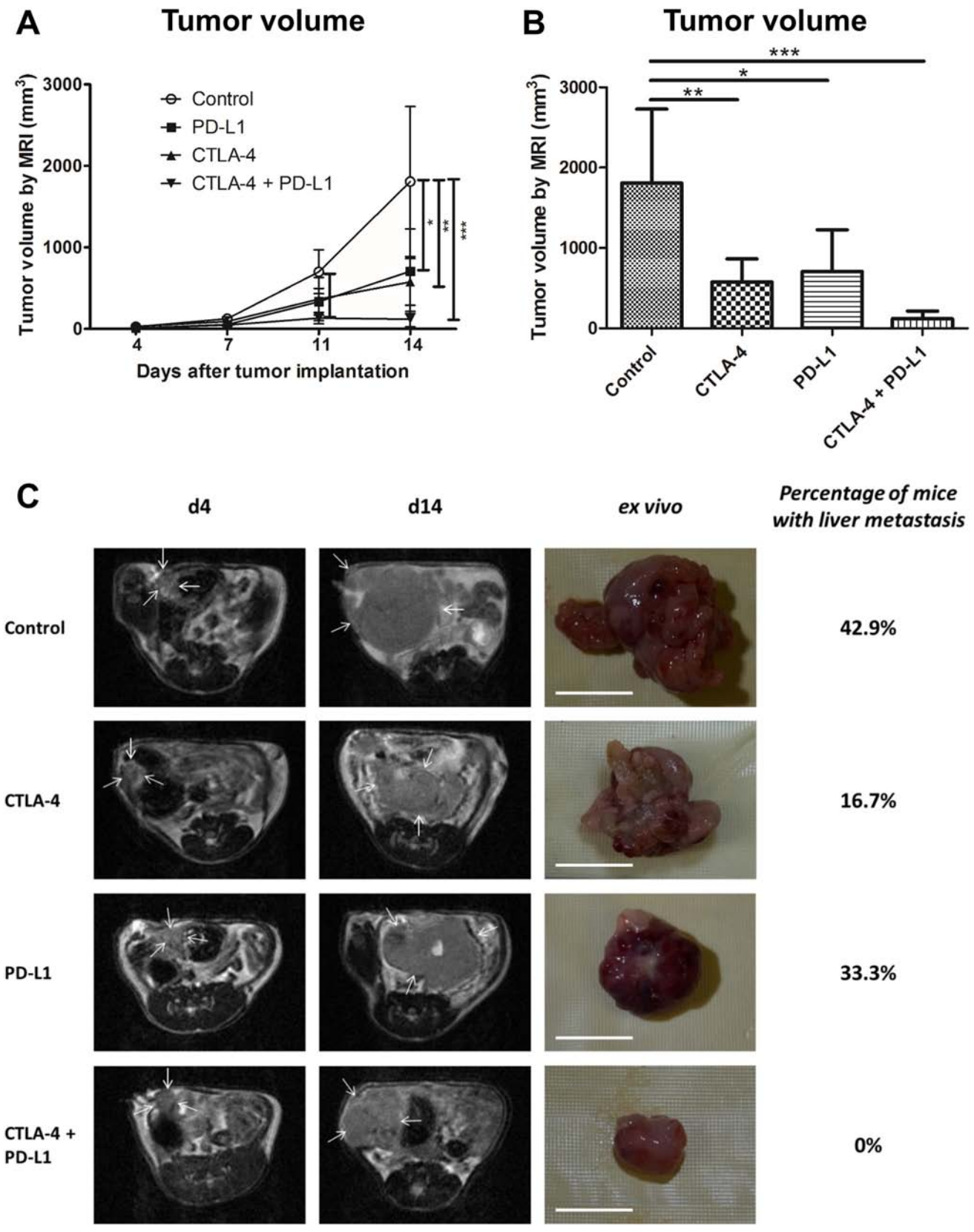


**Figure 1.** Dual CTLA-4 and PD-L1 blockade inhibits CT26 colon cancer growth. **A**, growth curves of orthotopically implanted CT26 tumors in mice that received IgG control, anti-CTLA-4, anti-PD-L1 antibodies or a combination of both (anti-CTLA-4 and anti-PD-L1), as determined by MR measurements. **B**, mean tumor volumes at day 14 p.i. displayed as bar chart. **C**, representative $T_2$-weighted MR images (first and second column) and images of excised colon tumors at day 14 p.i. (third column) confirm the smallest tumor sizes upon dual immune checkpoint blockade. Percentages of mice with liver metastases (fourth column) show inhibitory effects of immune checkpoint blockade on metastases. Data are presented as mean ± standard deviation. *$P < .05$, **$P < .01$, ***$P < .001$. Scale bar: 1 cm.

## Results

### *Combination Therapy with Anti-CTLA-4 and PDL-1 Antibodies Inhibits Colon Cancer Growth and Blocks Liver Metastasis*

The murine CT26 colon cancer cell line forms fast growing and highly vascularized tumors and the subcutaneous CT26 cancer model is frequently used for assessing the effects of therapeutic agents. Mutational analyses showed that the cell line is microsatellite stable and shows molecular characteristics of aggressive, undifferentiated, treatment-refractory, and metastasis-prone human colorectal carcinoma cells [19,29].

We have previously analyzed the effects of different anti-angiogenic drugs on growth and metastasis of orthotopically implanted CT26 tumors in nude mice [18]. Since immune checkpoint blockade has gained increasing interest for the treatment of advanced metastatic cancer, we transferred this model to syngeneic BALB/c mice and evaluated the effects of CTLA-4 and PD-L1 blockade as mono- and combination therapies.

All therapy regimens were well tolerated by the mice and no loss of body weight was measurable during the treatment period (Supplementary Figure S2).

Growth of the primary colon tumors was longitudinally investigated by $T_1$ and $T_2$-weighted MRI. Administration of either anti-PD-L1 or anti-CTLA-4 antibodies as monotherapies inhibited tumor growth, leading to significantly reduced mean tumor volumes at day 14 post-injection (p.i.). Combined PD-L1 and CTLA-4 blockade exerted stronger inhibitory effects than the monotherapies, as tumor growth almost stagnated upon therapy (d7 p.i.: $P < .05$, d11 and d14 p.i.: $P < .001$, Figure 1, *A* and *B*, exemplary MR images and images of excised tumors shown in C)).

As orthotopic CT26 tumor xenografts developed liver metastases in immunodeficient mice [18], we investigated the influence of the therapies on metastasis in the syngeneic colon cancer model by screening the livers macroscopically on day 14 p.i. after resection. In the control group, 43% of mice presented with liver metastases. The ratio was reduced to 33% of mice with liver metastases by anti-PD-L1 therapy. In the anti-CTLA-4 treatment group, liver metastases were found in 17% of the animals. In contrast, no liver metastases at all were detected after combination therapy with anti-CTLA-4 and anti-PD-L1 antibodies (Figure 1*C*).

### *Sole CTLA-4 and Dual Blockade of CTLA-4 and PD-L1 Increases Intratumoral CD4+ and CD8+ T Cells and Reduces FOXP3+ Treg Cells*

To investigate the mechanisms of tumor growth inhibition by immune checkpoint blockade, we analyzed the effects of the therapies on immune cells. Immunostaining and quantification of CD45 showed that the total amount of leucocytes was slightly higher in tumors of the anti-CTLA-4 monotherapy group and clearly lower in tumors of the anti-PD-L1 monotherapy group as compared to the control tumors. In tumors of the combination therapy group, the amount of CD45-positive leucocytes was comparable to the control tumors (Figure 2*A*).

Analysis of different T cell subtypes revealed that CD8+ and CD4+ T cells were significantly enhanced in tumors treated with anti-

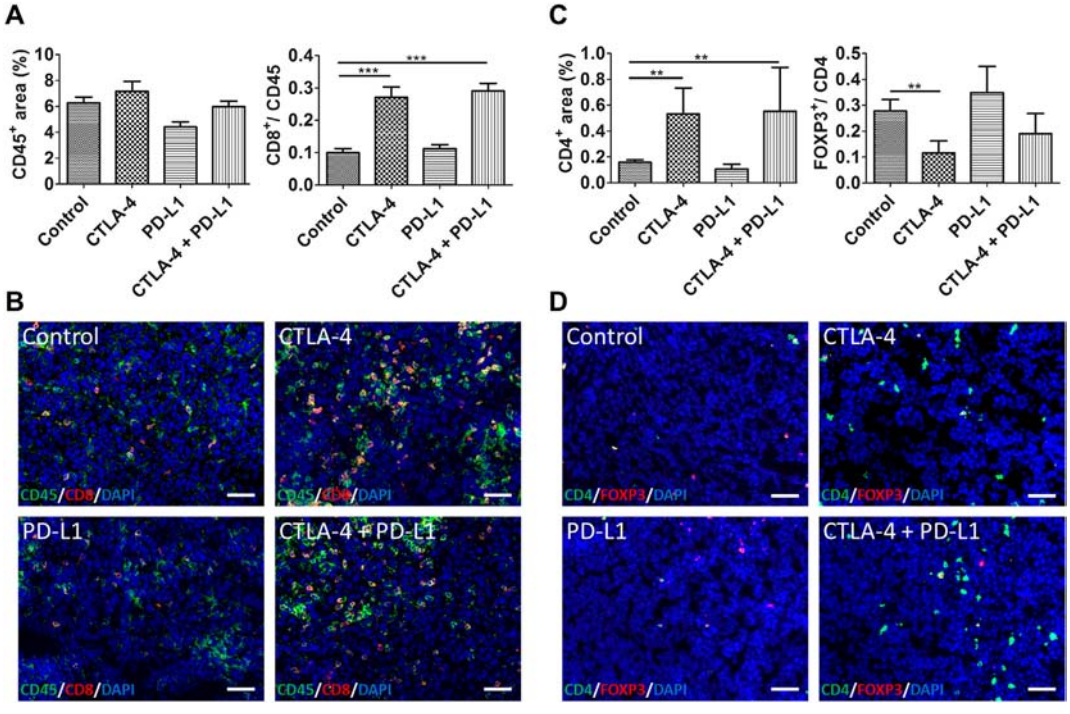


**Figure 2.** Sole CTLA-4 and dual CTLA-4 and PD-L1 blockade increase CD4+ and CD8+ T cells and reduce FOXP3+ Treg cells. Quantification of the CD45+ and CD8+ area fractions (**A**), the CD4+ (**C**) and the FOXP3/CD4 area fraction (**C**) at day 14 p.i. show no major alterations in the total leucocyte population after sole treatment with anti-CTLA-4 antibodies and combined treatment with anti-CTLA-4 and anti-PD-L1 antibodies (**A**), but a significant increase in CD8+ (**A**) and CD4+ T cells (**C**) as compared to control tumors, whereas intratumoral FOXP3+ Treg cells were reduced (**C**). All data are presented as mean ± standard deviation (*$P < .05$, ** $P < .01$, ***$P < .001$). Representative immunostainings for CD45 (**B**, green) and CD8 (**B**, red) as well as CD4 (**D**, green) and FOXP3 (**D,** red) of tumor sections from the different treatment groups at day 14 p.i. Counterstaining of cell nuclei by DAPI. Scale bars: 50 $\mu$m for all stainings.

CTLA-4 monotherapy and combination therapy group as compared to controls (CD8: $P < .001$ for both, CD4: $P < .05$ for both, Figure 2, *A* and *C*, exemplary immunofluorescent stainings shown in B and D). In contrast, sole PD-L1 blockade did not increase the intratumoral CD8+ T cells infiltrate.

In addition, single anti-CTLA-4 therapy significantly decreased the intratumoral FOXP3+/CD4+ Treg cells ($P < .01$). Combined anti-CTLA-4 and anti-PD-L1 treatment also reduced the intratumoral Treg cells, whereas in tumors of the anti-PD-L1 group, the amount of Treg cells was slightly higher than in the control tumors (Figure 2*C*, exemplary immunofluorescent stainings are shown in D).

### *Combination Blockade of CTLA-4 and PD-L1 Increases Intratumoral iNOS+ Macrophages and Reduces MRC1+, PD-L1+ and Tie2+ Macrophages (TEMs)*

Macrophages as most abundant leucocyte population within malignant tumors are important regulatory cells in the microenvironment [30,31]. Different polarization states have been described for macrophages, whereas M1 and M2 represent extremes within a broad range of activation states [30], and alterations in their polarization have been observed in response to anti-tumorigenic therapies [32].

Therefore, we analyzed the effects of our treatments on the macrophages in the colon tumors. Whereas the total amount of intratumoral macrophages was not altered after anti-CTLA-4 monotherapy and combined CTLA-4 and PD-L1 blockade, macrophages were reduced in tumors of animals receiving anti-PD-L1 monotherapy (Figure 3*A*).

Analysis of MRC1+ macrophages, a marker being associated with M2 polarization, revealed no major effects of sole CTLA-4 blockade. In tumors of the anti-PD-L1 monotherapy and the combination therapy group, however, the numbers of MRC1+ macrophages were significantly lower than in the control tumors ($P < .01$ and $P < .05$, respectively). Lowest numbers of MRC1+ macrophages were detected in tumors of the anti-PD-L1 monotherapy group (Figure 3*A*, representative immunostainings are shown in B).

The amount of iNOS+ macrophages, indicating polarization towards the M1 phenotype, was markedly higher in tumors of all therapy groups than in the controls. The increase in iNOS+ macrophages was stronger in the anti-CTLA-4 ($P < .05$) than the anti-PD-L1 monotherapy group. Highest numbers of iNOS+ macrophages were detected in the colon tumors of the combination therapy group ($P < .001$, Figure 3*C*, representative immunostainings are shown in D).

We analyzed PD-L1+ macrophages, because it has recently been shown that PD-L1+ macrophages play an immunosuppressive role in tumors and that inhibition of these macrophages is important for the efficacy of immune checkpoint blockade [32,33]. The amount of PD-L1+ macrophages was significantly reduced by all therapies as compared to the controls. Sole PD-L1 blockade ($P < .001$) led to a greater decrease in these macrophages than anti-CTLA-4 monotherapy ($P < .01$). Dual CTLA-4 and PD-L1 blockade induced the strongest reduction in intratumoral PD-L1+ macrophages ($P < .001$, Figure 3, *E* and *F*).

Since our previous results in the orthotopic CT26 xenograft colon cancer model pointed towards a crucial role of Tie2+ macrophages (TEMs) in metastasis of the primary tumors to the liver, we investigated the effects of the therapies on these macrophages [18]. The Tie2-positive area fraction in the tumors, which was calculated after manually excluding Tie2-positive vessels, thus being indicative for the amount of TEMs, was markedly decreased by sole PD-L1 blockade and by combined blockade of CTLA-4 and PD-L1. In contrast, blockade of CTLA-4 had no major effects on the intratumoral TEMs (Figure 3, *G* and *H*).

### *Dual CTLA-4 and PD-L1 Blockade does not Affect Vessel Functionality but Increases Fibroblast Accumulation*

We next investigated whether immune checkpoint blockade had additional effects on the tumor microenvironment besides inducing immune cell alterations. Recent studies have shown that activation of CD4+ T cells by immune checkpoint blockade can lead to enhanced vessel normalization [34]. Thus, the effects of immune checkpoint inhibition on tumor vascularization were longitudinally investigated using DCE-MRI. No major alterations in the amplitude A, a parameter of the relative blood volume, were detected in response to either sole or dual immune checkpoint inhibition, demonstrating that the functional vasculature was not affected by the immune therapies (Figure 4*A*). Immunohistological analyses of tumor sections at day 14 p.i. showed an increase in VEGFR2+ angiogenic microvessels in tumors of the combination therapy group as compared to the controls, though the differences were not significant (Figure 4*B*). In addition, mature microvessels, detected via SMA, were decreased upon all therapies. The lowest amount of mature microvessels in tumors was detected after combined anti-CTLA-4 and anti-PD-L1 treatment ($P < .01$, Figure 4*C*).

Analysis of further stromal alterations revealed that both, PDGFR-β+ and FAP+ cells, were significantly enhanced in tumors of the combination therapy group as compared to the control tumors ($P < .001$ for both), showing an increase in intratumoral fibroblasts. No significant changes in fibroblast accumulation were observed after anti-PD-L1 monotherapy. Sole CTLA-4 blockade increased the amount of PDGFR-β+ ($P < .01$) but slightly decreased FAP+ cells (Figure 4*D*, representative immunostainings of PDGFR-β+ cells are shown in E). In addition, in line with the stronger accumulation of fibroblasts, combined immune checkpoint inhibition led to a slight increase in collagen IV and a significant enhancement of collagen I deposition as compared to control tumors ($P < .05$, Figure 4*F*, immunostainings for Col I are shown in G).

### *Combination Therapy Leads to Alterations in Inflammation Associated Cytokines, Angiogenesis and Stroma-Related Factors*

In view of the cellular changes that were observed in the tumor microenvironment in response to the therapies, we further analyzed the tumors for the expression of cytokines, enzymes and growth factors that are associated with inflammation or involved in angiogenesis and stromal activation.

First, we assessed the expression of pro-inflammatory cytokines, such as IL-1α, IFN-γ, IL-2 and IL-12, which are associated with activation of CD8+ cytotoxic T cells, Th1 response of T-cells, M1 polarization of macrophages and an anti-tumorigenic immune response. IL-1α and IFN-γ mRNA were markedly up-regulated in tumors of the CTLA-4 monotherapy and the combination therapy group, whereas there was no increase in the PD-L1 monotherapy group (Supplementary Figure S3). This was confirmed at the protein level, however, the increase was stronger in tumors of the anti-CTLA-4 monotherapy group (IL-1α: $P < .001$, IFN-γ: $P < .05$; Figure 5*A*). Expression of IL-2 mRNA and protein was significantly enhanced in tumors upon anti-CTLA-4 monotherapy ($P < .001$) and slightly increased after combination therapy (Figure 5*A* and

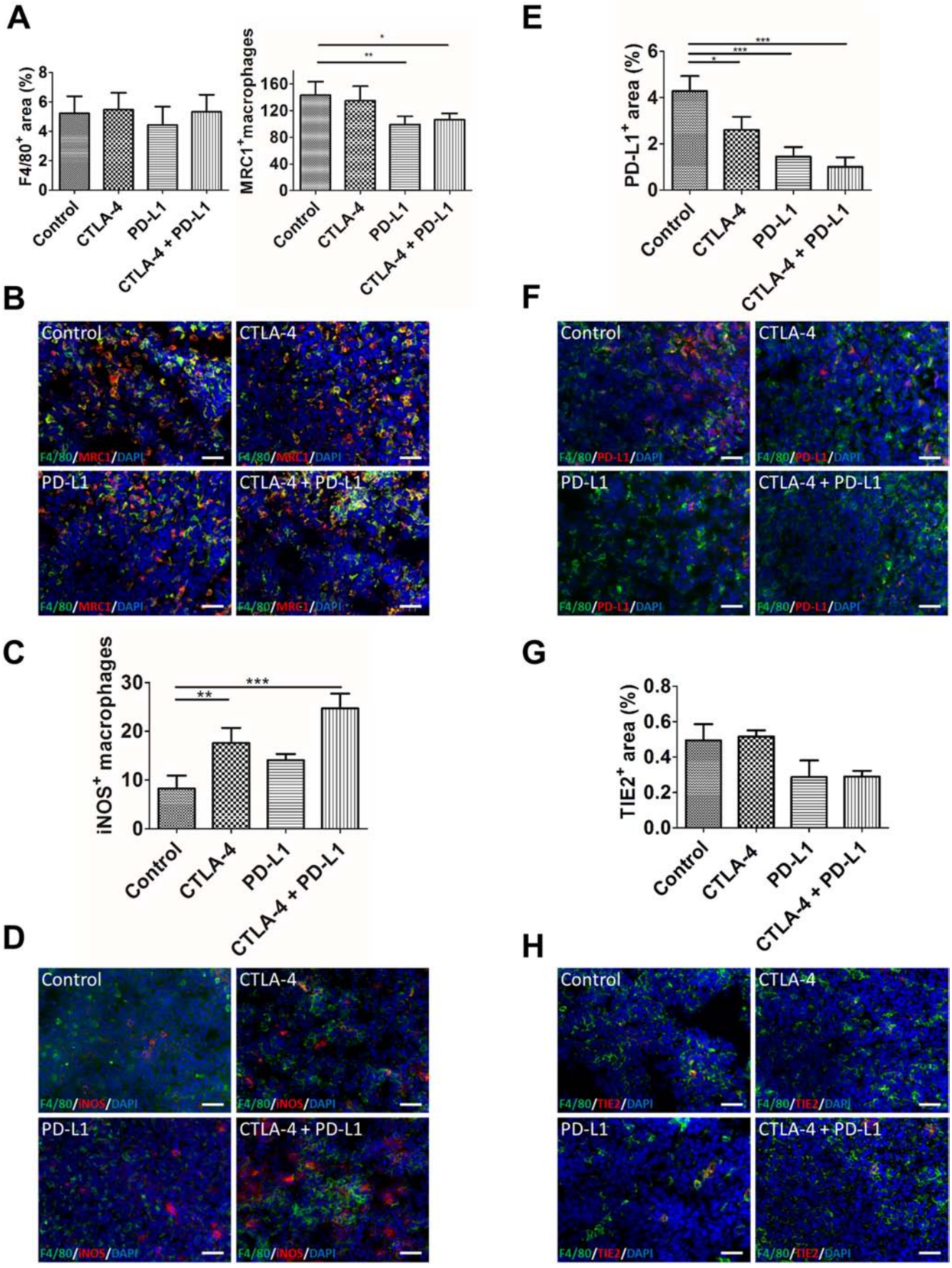
A
F4/80+ area (%)
MRC1+macrophages
Control
CTLA-4
PD-L1
CTLA-4 + PD-L1
E
PD-L1+ area (%)
B
F
C
iNOS+ macrophages
G
TIE2+ area (%)
D
H
F4/80/MRC1/DAPI
F4/80/PD-L1/DAPI
F4/80/iNOS/DAPI
F4/80/TIE2/DAPI

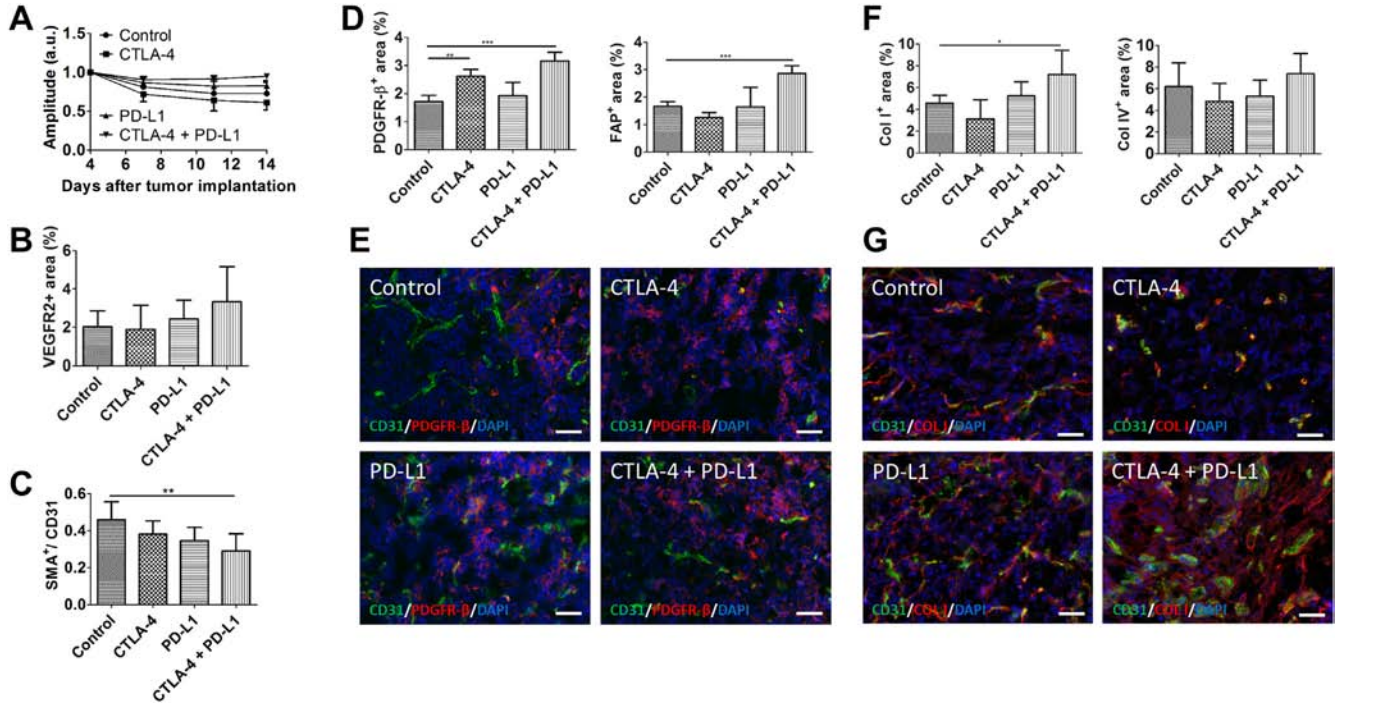


**Figure 4.** Microenvironmental changes after dual CTLA-4 and PD-L1 blockade. **A**, DCE-MRI data indicating that the amplitude A (a parameter of the relative blood distribution volume of the tumor) does not significantly change during the different treatments. **B**, analysis of the angiogenic activity in tumors of the different treatment groups as determined by the ratio of the VEGFR2 + to the CD31+ area fraction. **C**, vessel maturation is decreased upon all therapies as shown by quantification of SMA+ vessels. **D**, the area fractions of PDGFR-β (left) and FAP (right) are significantly enhanced in tumors of the combined treatment group. **E**, representative immunostainings for CD31 (vessels, green), PDGFR-β (red) and DAPI (cell nuclei, blue) of the different treatment groups. **F**, dual immune checkpoint blockade leads to an increase in the Col I (left) and Col IV (right) + area fraction. **G**, representative stainings for Col I (red), CD31 (green) and DAPI (cell nuclei, blue) in tumor section at day 14 p.i. Data are presented as mean ± standard deviation (*$P < .05$, **$P < .01$, ***$P < .001$). Scale bars: 50 $\mu$m for all staining.

Supplementary Figure S3). IL-12 mRNA was up-regulated by all therapies (Supplementary Figure S3). At the protein level, IL-12 levels were highest in tumors of the anti-CTLA-4 monotherapy group (Figure 5*A*, $P < .001$). A minor increase was also detected in tumors of the combination therapy group (Figure 5*A*). These analyses point to a shift towards pro-inflammatory Th1 and M1 like phenotypes associated with an anti-tumorigenic immune response after anti-CTLA-4 and combination therapy.

In addition, we analyzed the expression of cytokines and enzymes related with Th2 response of T-cells and M2 polarization of macrophages like IL-4, thymus and activation regulated chemokine (TARC), cyclooxygenase-2 (COX-2) and arginase-1 (ARG1), being indicative for a tumor-promoting phenotype of the immune microenvironment. We detected lower expression of IL-4, TARC and COX-2 protein in tumors of the PD-L1 monotherapy group than in the control tumors. Lowest levels were recorded for the combination therapy group (Figure 5*B*, COX-2: $P < .001$, IL-4: $P < .05$). In tumors of the CTLA-4 monotherapy group, IL-4 protein expression was only slightly decreased, COX-2 protein levels were almost similar as in the control tumors, whereas TARC levels were even enhanced (Figure 5*B*). At the mRNA level, IL-4, TARC, COX-2 and ARG1 expression was also lowest in tumors of the combination therapy group. On the other hand, these tumors showed highest iNOS mRNA expression, a marker of M1 polarized macrophages ($P < .05$, Supplementary Figure S3). These results showing a reduction in M2 and Th2 related factors are in line with the

**Figure 3.** Sole PD-L1 and dual CTLA-4 and PD-L1 inhibition alter macrophage phenotypes. **A**, quantification of the F4/80+ area fraction (left) reveals a slightly lower amount of macrophages after anti-PD-L1 treatment. The number of MRC1+ macrophages (right, counted manually), is significantly reduced in the anti-PD-L1 and combined treatment groups. **B**, representative immunostainings for F4/80 (green) and MRC1 (red) of tumor sections from the different treatment groups at day 14 p.i. **C**, quantification of immunostainings shows significantly higher numbers of iNOS+ macrophages (counted manually) in tumors after sole CTLA-4 and dual CTLA-4 and PD-L1 inhibition as compared to control tumors. **D**, representative immunostainings for F4/80 (green) and iNOS (red) of tumor sections at day 14 p.i. **E**, quantification of PD-L1+ macrophages on tumor sections at day 14 p.i. reveals a significant decrease in intratumoral PD-L1+ macrophages after all therapies in comparison to the controls. Lowest numbers of PD-L1+ macrophages are seen in tumors of the combined treatment group. **F**, exemplary immunofluorescent stainings for F4/80 (green) and PD-L1 (red). **G**, Tie2+ macrophages are lower in tumors after anti-PD-L1 and combinatorial treatment as compared to the control tumors, as determined by immunostaining of tumor sections for F4/80 (**H** green) and Tie2 (**H**, red). Cell nuclei are counterstained with DAPI (blue) for all stainings. Data are presented as mean ± standard deviation (*$P < .05$, **$P < .01$, ***$P < .001$). Scale bars: 50 $\mu$m for all stainings.

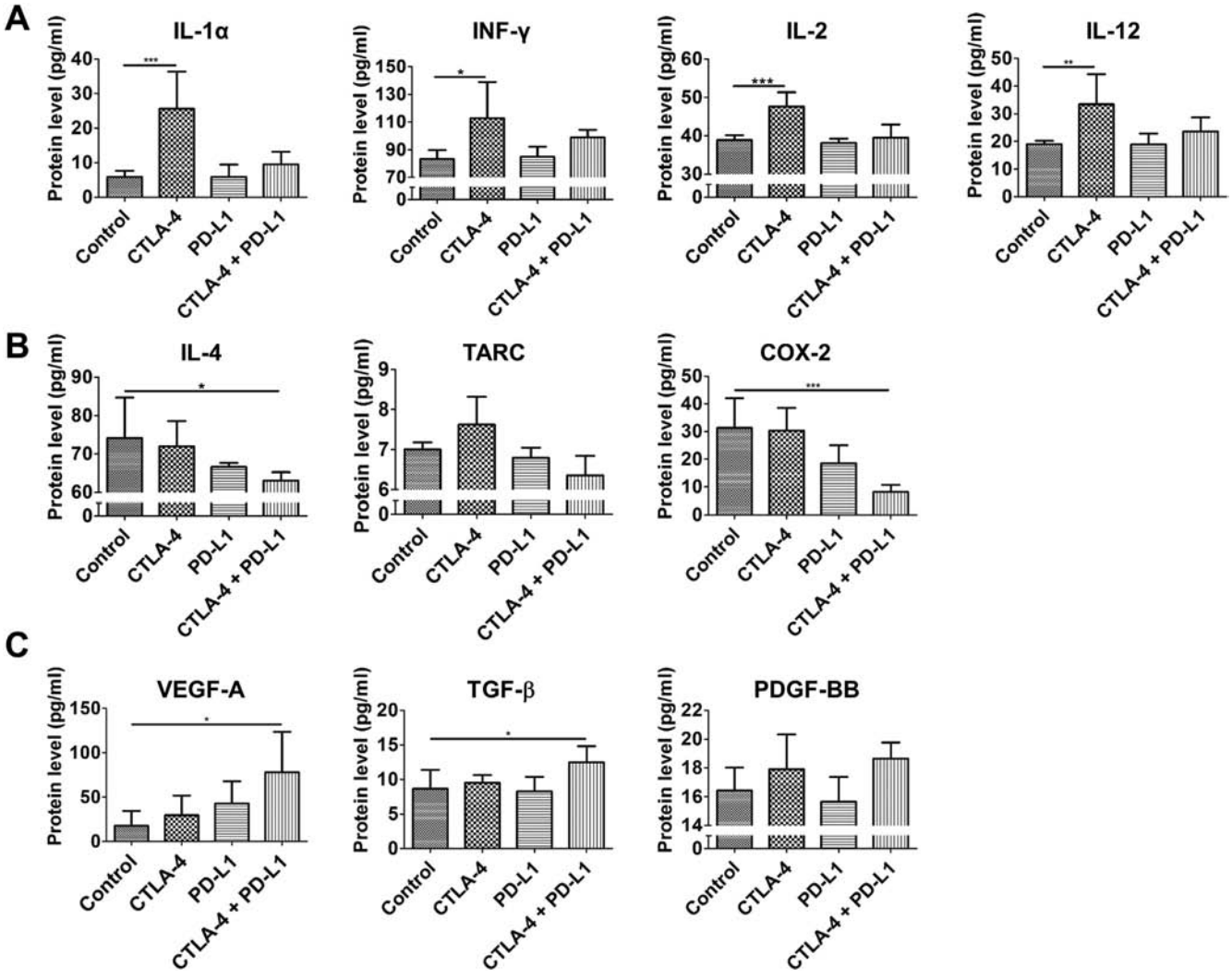


**Figure 5.** Dual CTLA-4 and PD-L1 blockade increases the expression of Th1/M1 associated cytokines, decreases the expression of Th2/M2 related cytokines, chemokines and enzymes and increases stromal factors. Analysis of the expression of Th1/M1 (**A**), M2/Th2 (**B**) and stroma **(C)** associated proteins in tumors of the different treatments groups at day 14 p.i. by ELISA. Data are presented as mean ± standard deviation (*$P < .05$, **$P < .01$, ***$P < .001$).

immunohistochemical data on intratumoral macrophage populations and further indicate a shift towards M1 polarization of macrophages associated with a Th1 response after dual CTLA-4 and PD-L1 blockade.

Analysis of pro-angiogenic and stroma related growth factors revealed that VEGF-A mRNA and protein levels were increased in response to all therapies. Highest intratumoral VEGF-A levels were detected after dual CTLA-4 and PD-L1 blockade (Figure 5*C* and Supplementary Figure S3, $P < .05$ (both, mRNA and protein)). We further analyzed the expression of TGF-β, PDGF-BB and PDGFR-β, which are involved in stromal activation and the fibrotic response mediated by tumor-associated fibroblasts. Tumors of the combination therapy group showed the highest expression of TGF-β ($P < .05$) and PDGF-B mRNA and protein as well as the highest levels of PDGFR-β mRNA (Figure 5*C* and Supplementary Figure S3). These results suggest slight pro-angiogenic effects and the induction of a fibrotic response by combined CTLA-4 and PD-L1 inhibition.

## Discussion

Immune checkpoint blockade has improved progression-free survival in patients with microsatellite instable/ mismatch repair deficient CRCs in clinical studies leading to an accelerated approval. However, microsatellite-instable and repair deficient CRCs represent only a minority, and for the majority of CRCs, immune checkpoint inhibitors as monotherapies have shown only limited efficacy in patients so far [11,12], emphasizing the need for further research to better understand the potential and limitations of these therapies. Anti-CTLA-4, anti-PD-1 and anti-PD-L1 antibodies act differentially on the immune cells [35] and recent studies have shown that their mechanisms of action can go beyond the activation of effector T cells and reduction of Treg cells [36–38]. We therefore investigated the effects of anti-CTLA-4 and anti-PD-L1 antibodies as mono- and combination therapies on the progression of syngeneic, orthotopically implanted microsatellite-stable colon carcinomas.

Longitudinal MR measurements for 11 days and screening of livers ex vivo showed that combined CTLA-4 and PD-L1 blockade led

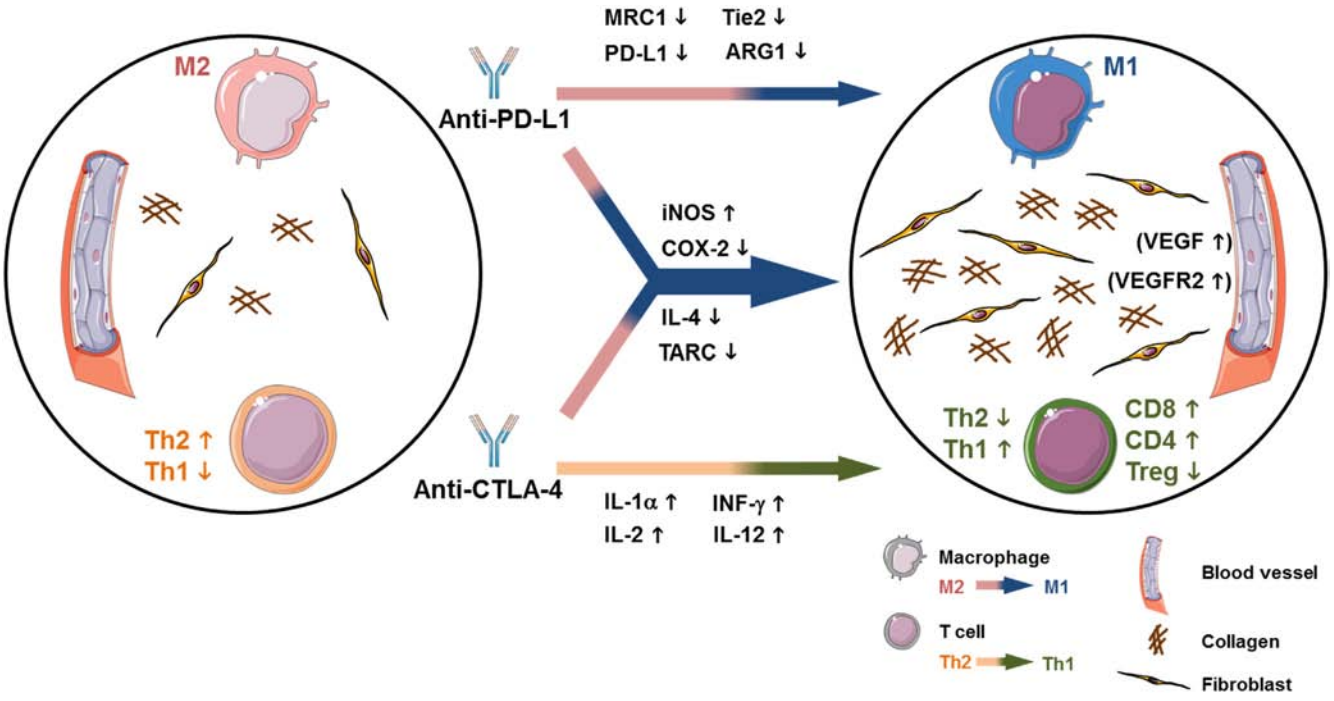


**Figure 6.** Suggested mechanism of the synergistic inhibitory effects of dual CTLA-4 and PD-L1 blockade on growth and metastasis of the orthotopic CT26 colon tumors. Anti-CTLA-4 antibodies lead to an increase in CD8+ and CD4+ T cells and a decrease in Treg cells accompanied by a pro-inflammatory Th1 response associated with increased expression of IL-1α, IFN-γ, IL-2, and IL-12. PD-L1 blockade induces a switch to pro-inflammatory M1 macrophages associated with decreased MRC-1, PD-L1, Tie2 and ARG1 expression. Additional synergistic effects of combined CTLA-4 and PD-L1 blockade on the immune microenvironment are obvious by the strongest increase in iNOS expression and the strongest reduction in COX-2, IL-4 and TARC expression. Moreover, dual immune checkpoint blockade induces a stromal reaction with significantly increased fibroblast accumulation and collagen deposition and a slight increase in VEGF-A and VEGFR2 expression which can either indicate stable disease or a compensatory reaction of the tumor to induce therapy resistance. This figure was created with images adapted from Servier Medical Art by Servier. Original images are licensed under a Creative Commons Attribution 3.0 Unported License.

almost to tumor growth stagnation and completely inhibited liver metastasis. Monotherapies with the respective antibodies exerted lower anti-tumorigenic effects, though sole CTLA-4 blockade was superior to anti-PD-L1 monotherapy. These results demonstrated synergistic inhibitory effects of dual antibody therapy on tumor growth and liver metastasis.

Further analyses revealed major effects of anti-CTLA-4 and combined anti-CTLA-4 and anti-PD-L1 therapy on T cells. In both treatment groups, intratumoral CD8+ and CD4+ T cells were significantly increased, whereas FOXP3+ Treg cells were significantly reduced as compared to the control group. Since the anti-CTLA-4 monotherapy and the combination treatment induced comparable alterations in CD8+ and CD4+ T cell subpopulations, we conclude that the effects on T cells can mainly be attributed to the CTLA-4 blockade. This is further sustained by the highest levels of IFN-γ, IL-2, IL-1α and IL-12 in tumors of the anti-CTLA-4 monotherapy group. These pro-inflammatory, Th1-related cytokines are associated with activation of CD8+ cytotoxic T cells and an anti-tumorigenic immune response (Figure 6) [39,40]. However, the stronger effects of sole CTLA-4 blockade on Treg cells and Th1 cytokine expression in our orthotopic colon cancer model differ from findings obtained in subcutaneous CT26 tumors. Duraiswamy and colleagues observed more pronounced T cell alterations upon dual CTLA-4 and PD-L1 inhibition than by sole CTLA-4 blockade [14]. This discrepancy could be attributed to a different microenvironment in intestinal and subcutaneous tissue. Zhao and colleagues recently showed that the number of T cells is higher in orthotopic than subcutaneous colon tumors, associated with enhanced levels of pro-inflammatory cytokines (e.g. IL-2, IFN-γ), thus resulting in a higher sensitivity of the orthotopic tumors to immune checkpoint inhibitors [17]. This could explain why sole CTLA-4 blockade which primarily acts on T cells had already maximal effects on T cells in our orthotopic CRC model that could not be outperformed by dual checkpoint inhibition.

However, since sole CTLA-4 blockade had similar or even stronger effects on T cells than the combination therapy, T cells were obviously not the sole key mediators of tumor growth and metastasis inhibition upon dual immune checkpoint blockade. Interestingly, combination therapy as well as anti-PD-L1 monotherapy induced major alterations in macrophage phenotypes. Strongest effects were observed after dual checkpoint blockade, as obvious by the significantly reduced numbers of MRC1+ macrophages, the lowest amount of PD-L1+ macrophages and the highest numbers of iNOS+ macrophages. These observations indicated a shift from pro-tumorigenic M2 towards anti-tumorigenic and pro-inflammatory M1 polarized macrophages which was further sustained by the lowest expression of the M2/ Th2 related factors IL-4, TARC, COX-2 and ARG1 (Figure 6).

Macrophages are the most abundant immune cells in carcinomas. They have important regulatory functions and the ability to control the immune response. However, whereas the effects of immune

checkpoint blockade on T cells are well recognized, it has only recently become evident that immune checkpoint inhibitors, mainly of the PD1-/PD-L1 pathway, can also act on antigen-presenting cells such as macrophages or dendritic cells and that these immune cells are important for the effectiveness of immune checkpoint blockade. In this context, Lin and colleagues found strong expression of functional PD-L1 in tumor-associated macrophages and dendritic cells and could demonstrate that host PD-L1 but not tumor cell PD-L1 was crucial for the efficacy of PD-L1 inhibition [32]. In addition, the authors found a correlation between PD-L1 expression on these immune cells in human ovarian cancer and melanoma and the effectiveness of anti-PD-1 monotherapy and combination blockade with anti-PD-1 and anti-CTLA-4 antibodies, respectively, suggesting that PD-L1 expression on tumor macrophages and dendritic cells may be predictive for the efficacy of these treatments [32].

Saha et al. investigated the effects of dual immune checkpoint inhibition combined with oncolytic virus therapy in mouse gliomas. Although triple combination therapy was most effective, dual checkpoint blockade (anti-PD-1 and anti-CTLA-4) already increased intratumoral CD8+ T cells, and slightly iNOS+ macrophages, whereas PD-L1+ macrophages were reduced, resulting in an increased median survival rate of 37% [36]. The authors could further demonstrate that the therapeutic efficacy of the combination therapy depended on all, CD4+ and CD8+ T cells as well as on macrophages. These findings are in line with our observations in the orthotopic colon cancer model demonstrating synergistic effects of CTLA-4 and PD-L1 blockade on T cells and macrophages, thus leading to efficient inhibition of cancer growth and metastasis.

Interestingly, sole PD-L1 inhibition and combination therapy also reduced the accumulation of TEMs in the tumors. TEMs comprise a special subpopulation of macrophages with high proangiogenic activity that express M2 polarization markers and play a crucial role in the metastatic spread of cancer cells. They are often located in close proximity to tumoral blood vessels and were shown to facilitate cancer cell intravasation and dissemination by releasing VEGF that transiently enhances vessel permeability [41–43]. In addition, immunosuppressive functions have been described for TEMs [44,45]. The results from our previous studies obtained in the orthotopic CT26 xenograft colon cancer model strongly suggested a crucial role of these macrophages in driving metastasis of the primary colon cancer cells to the liver [18]. Now we confirm the presence of these macrophages in the syngeneic orthotopic CT26 colon tumors. Moreover, we provide evidence that recruitment of these Tie2+ macrophages to the colon tumors can be inhibited by anti-PD-L1 and dual immune checkpoint blockade which further underlines their supportive role in metastasis of the colon cancer cells to the liver. We assume that inhibition of TEMs can be ascribed to PD-L1 blockade since TEM accumulation was not reduced in tumors of the anti-CTLA-4 monotherapy group and the reduction was similar in the PD-L1 monotherapy and combination therapy group. However, further studies are needed in order to decipher the effects of the immune checkpoint inhibitors on TEMs and the other macrophage subpopulations.

Immune checkpoint blockade has recently been described to enhance vessel normalization by activating CD4+ T cells and inducing a Th1 response [34]. However, in the orthotopic CT26 colon cancer model, we did not observe an increase in vessel normalization in response to sole or dual immune checkpoint inhibition. Immunohistological analyses revealed significantly lower vessel maturation, an increase in VEGFR2-positive angiogenic microvessels and significantly enhanced VEGF-A levels after dual CTLA-4 and PD-L1 blockade (Figure 6). Nevertheless, no major alterations in the amplitude A, a parameter of the relative blood volume, were measured by DCE-MRI, demonstrating that these changes were restricted to the microvessels and that the functional vasculature was not influenced by either sole or dual immune checkpoint inhibition. Moreover, combination therapy induced a stromal reaction, as obvious by the significant accumulation of PDGFR-β + and FAP+ fibroblasts and strong deposition of collagen I in the colon carcinomas (Figure 6). Tumor-associated fibroblasts have been shown to promote angiogenesis by secreting VEGF-A and other cytokines and chemokines as well as matrix metalloproteinases which may provide an explanation for the increase in VEGFR2-positive angiogenic microvessels [46,47]. However, contradictory observations have been made with regard to their role in cancer progression. On the one hand, tumor-promoting functions of fibroblasts have been described (e.g., by facilitating cancer cell invasion, by stimulating tumor angiogenesis and by modulating tumor immunity), they have been identified as mediators of drug resistance and are currently discussed to be involved in resistance towards immune checkpoint blockade [46]. On the other hand, activation of fibroblasts can be induced as a defense mechanism in order to impair cancer progression. Recently, fibroblasts have been shown to inhibit cancer progression in a mouse model of pancreatic ductal adenocarcinoma, and depletion of these cells resulted in a diminished survival of the tumor-bearing mice [48]. Whether the stromal response induced in the orthotopic colon tumors upon dual immune checkpoint inhibition reflects stable disease due to efficient immunotherapy or is rather indicative for a compensatory mechanism of the tumor to induce therapy resistance needs further investigation.

In conclusion, our findings show that dual CTLA-4 and PD-L1 blockade exert synergistic inhibitory effects on growth and metastasis of the orthotopic CT26 colon tumors by increasing CD8+ and CD4+ T cells associated with a Th1 response mediated by CTLA-4 inhibition and by inducing a shift towards M1 macrophage polarization, which can mostly be ascribed to PD-L1 blockade. The pronounced stromal response observed after dual immune checkpoint blockade underlines that the effects of immune checkpoint inhibition go beyond immune cell modulation and highlights the link between immunomodulation and desmoplasia.

## Appendix A. Supplementary data

Supplementary data to this article can be found online at https://doi.org/10.1016/j.neo.2019.07.006.

## References

[1] Siegel RL, Miller KD, and Jemal A (2018). Cancer statistics, 2018. *CA Cancer J Clin* **68**(1), 7–30. doi:10.3322/caac.21442.

[2] Kuipers EJ, Grady WM, Lieberman D, Seufferlein T, Sung JJ, Boelens PG, van de Velde CJ, and Watanabe T (2015). Colorectal cancer. *Nat Rev Dis Primers* **1**, 15065. doi:10.1038/nrdp.2015.65.

[3] Martini G, Troiani T, Cardone C, Vitiello P, Sforza V, Ciardiello D, Napolitano S, Della Corte CM, Morgillo F, and Raucci A, et al (2017). Present and future of metastatic colorectal cancer treatment: A review of new candidate targets. *World J Gastroenterol* **23**(26), 4675–4688. doi:10.3748/wjg.v23.i26.4675.

[4] Seow HF, Yip WK, and Fifis T (2016). Advances in targeted and immunobased therapies for colorectal cancer in the genomic era. *Onco Targets Ther* **9**, 1899–1920. doi:10.2147/OTT.S95101.

[5] Passardi A, Canale M, Valgiusti M, and Ulivi P (2017). Immune Checkpoints as a Target for Colorectal Cancer Treatment. *Int J Mol Sci* , 18(6). doi:10.3390/ijms18061324.

[6] Pardoll DM (2012). The blockade of immune checkpoints in cancer immunotherapy. *Nat Rev Cancer* **12**(4), 252–264. doi:10.1038/nrc3239.

[7] Singh PP, Sharma PK, Krishnan G, and Lockhart AC (2015). Immune checkpoints and immunotherapy for colorectal cancer. *Gastroenterol Rep (Oxf)* **3** (4), 289–297. doi:10.1093/gastro/gov053.

[8] Sharma P and Allison JP (2015). The future of immune checkpoint therapy. *Science* **348**(6230), 56–61. doi:10.1126/science.aaa8172.

[9] Nishikawa H and Sakaguchi S (2010). Regulatory T cells in tumor immunity. *Int J Cancer* **127**(4), 759–767. doi:10.1002/ijc.25429.

[10] Francisco LM, Salinas VH, Brown KE, Vanguri VK, Freeman GJ, Kuchroo VK, and Sharpe AH (2009). PD-L1 regulates the development, maintenance, and function of induced regulatory T cells. *J Exp Med* **206**(13), 3015–3029. doi:10.1084/jem.20090847.

[11] Le DT, Uram JN, Wang H, Bartlett BR, Kemberling H, Eyring AD, Skora AD, Luber BS, Azad NS, and Laheru D, et al (2015). PD-1 Blockade in Tumors with Mismatch-Repair Deficiency. *N Engl J Med* **372**(26), 2509–2520. doi:10.1056/NEJMoa1500596.

[12] Boland PM and Ma WW (2017). Immunotherapy for Colorectal Cancer. *Cancers (Basel)* , 9(5). doi:10.3390/cancers9050050.

[13] Yu G, Wu Y, Wang W, Xu J, Lv X, Cao X, and Wan T (2018). Low-dose decitabine enhances the effect of PD-1 blockade in colorectal cancer with microsatellite stability by re-modulating the tumor microenvironment. *Cell Mol Immunol* . doi:10.1038/s41423-018-0026-y.

[14] Duraiswamy J, Kaluza KM, Freeman GJ, and Coukos G (2013). Dual blockade of PD-1 and CTLA-4 combined with tumor vaccine effectively restores T-cell rejection function in tumors. *Cancer Res* **73**(12), 3591–3603. doi:10.1158/0008-5472.CAN-12-4100.

[15] Li J, Xu J, Yan X, Jin K, Li W, Zhang R. Targeting Interleukin-6 (IL-6) Sensitizes Anti-PD-L1 Treatment in a Colorectal Cancer Preclinical Model. Medical science monitor : international medical journal of experimental and clinical research **2018**;24:5501–8 doi 10.12659/msm.907439.

[16] Lewis KE, Selby MJ, Masters G, Valle J, Dito G, Curtis WR, Garcia R, Mink KA, Waggie KS, and Holdren MS, et al (2017). Interleukin-21 combined with PD-1 or CTLA-4 blockade enhances antitumor immunity in mouse tumor models. *Oncoimmunology* **7**(1)e1377873. doi:10.1080/2162402X.2017.1377873.

[17] Zhao X, Li L, Starr TK, Subramanian S. Tumor location impacts immune response in mouse models of colon cancer. Oncotarget **2017**;8(33):54775–87 doi 10.18632/oncotarget.18423.

[18] Abou-Elkacem L, Arns S, Brix G, Gremse F, Zopf D, Kiessling F, and Lederle W (2013). Regorafenib inhibits growth, angiogenesis, and metastasis in a highly aggressive, orthotopic colon cancer model. *Mol Cancer Ther* **12**(7), 1322–1331. doi:10.1158/1535-7163.MCT-12-1162.

[19] Castle JC, Loewer M, Boegel S, de Graaf J, Bender C, Tadmor AD, Boisguerin V, Bukur T, Sorn P, and Paret C, et al (2014). Immunomic, genomic and transcriptomic characterization of CT26 colorectal carcinoma. *BMC Genomics* **15** (1), 190. doi:10.1186/1471-2164-15-190.

[20] Hoffman RM (1999). Orthotopic metastatic mouse models for anticancer drug discovery and evaluation: a bridge to the clinic. *Invest New Drugs* **17**(4), 343–359.

[21] Gremse F, Stark M, Ehling J, Menzel JR, Lammers T, and Kiessling F (2016). Imalytics preclinical: interactive analysis of biomedical volume data. *Theranostics* **6**(3), 328–341. doi:10.7150/thno.13624.

[22] Kiessling F, Jugold M, Woenne EC, and Brix G (2007). Non-invasive assessment of vessel morphology and function in tumors by magnetic resonance imaging. *Eur Radiol* **17**(8), 2136–2148. doi:10.1007/s00330-006-0566-x.

[23] Brix G, Semmler W, Port R, Schad LR, Layer G, and Lorenz WJ (1991). Pharmacokinetic parameters in CNS Gd-DTPA enhanced MR imaging. *J Comput Assist Tomogr* **15**(4), 621–628.

[24] Port RE, Knopp MV, Hoffmann U, Milker-Zabel S, and Brix G (1999). Multicompartment analysis of gadolinium chelate kinetics: blood-tissue exchange in mammary tumors as monitored by dynamic MR imaging. *Journal of magnetic resonance imaging : JMRI* **10**(3), 233–241.

[25] Doleschel D, Rix A, Arns S, Palmowski K, Gremse F, Merkle R, Salopiata F, Klingmüller U, Jarsch M, and Kiessling F, et al (2015). Erythropoietin improves the accumulation and therapeutic effects of carboplatin by enhancing tumor vascularization and perfusion. *Theranostics* **5**(8), 905–918. doi:10.7150/thno.11304.

[26] Boaru SG, Borkham-Kamphorst E, Tihaa L, Haas U, Weiskirchen R. Expression analysis of inflammasomes in experimental models of inflammatory and fibrotic liver disease. Journal of inflammation (London, England) **2012**;9(1):49 doi https://doi.org/10.1186/1476-9255-9-49.

[27] Schmittgen TD and Livak KJ (2008). Analyzing real-time PCR data by the comparative C(T) method. *Nat Protoc* **3**(6), 1101–1108.

[28] Borkham-Kamphorst E, Steffen BT, van de Leur E, Haas U, and Weiskirchen R (2018). Portal myofibroblasts are sensitive to CCN-mediated endoplasmic reticulum stress-related apoptosis with potential to attenuate biliary fibrogenesis. *Cell Signal* **51**, 72–85. doi:10.1016/j.cellsig.2018.07.005.

[29] Castle JC, Loewer M, Boegel S, Tadmor AD, Boisguerin V, de Graaf J, Paret C, Diken M, Kreiter S, and Türeci Ö, et al (2014). Mutated tumor alleles are expressed according to their DNA frequency. *Sci Rep* **4**, 4743. doi:10.1038/srep04743.

[30] Solinas G, Germano G, Mantovani A, and Allavena P (2009). Tumor-associated macrophages (TAM) as major players of the cancer-related inflammation. *J Leukoc Biol* **86**(5), 1065–1073. doi:10.1189/jlb.0609385.

[31] Noy R and Pollard JW (2014). Tumor-associated macrophages: from mechanisms to therapy. *Immunity* **41**(1), 49–61. doi:10.1016/j.immuni.2014.06.010.

[32] Lin H, Wei S, Hurt EM, Green MD, Zhao L, Vatan L, Szeliga W, Herbst R, Harms PW, and Fecher LA, et al (2018). Host expression of PD-L1 determines efficacy of PD-L1 pathway blockade-mediated tumor regression. *J Clin Invest* **128**(2), 805–815. doi:10.1172/JCI96113.

[33] Prima V, Kaliberova LN, Kaliberov S, Curiel DT, and Kusmartsev S (2017). COX2/mPGES1/PGE2 pathway regulates PD-L1 expression in tumor-associated macrophages and myeloid-derived suppressor cells. *Proc Natl Acad Sci U S A* **114**(5), 1117–1122. doi:10.1073/pnas.1612920114.

[34] Tian L, Goldstein A, Wang H, Ching Lo H, Sun Kim I, Welte T, Sheng K, Dobrolecki LE, Zhang X, and Putluri N, et al (2017). Mutual regulation of tumour vessel normalization and immunostimulatory reprogramming. *Nature* **544**(7649), 250–254. doi:10.1038/nature21724.

[35] Twyman-Saint Victor C, Rech AJ, Maity A, Rengan R, Pauken KE, Stelekati E, Benci JL, Xu B, Dada H, and Odorizzi PM, et al (2015). Radiation and dual checkpoint blockade activate non-redundant immune mechanisms in cancer. *Nature* **520**(7547), 373–377. doi:10.1038/nature14292.

[36] Saha D, Martuza RL, and Rabkin SD (2017). Macrophage Polarization Contributes to Glioblastoma Eradication by Combination Immunovirotherapy and Immune Checkpoint Blockade. *Cancer Cell* **32**(2), 253–267 e5 https://doi.org/10.1016/j.ccell.2017.07.006.

[37] Tang H, Liang Y, Anders RA, Taube JM, Qiu X, Mulgaonkar A, Liu X, Harrington SM, Guo J, and Xin Y, et al (2018). PD-L1 on host cells is essential for PD-L1 blockade-mediated tumor regression. *J Clin Invest* **128**(2), 580–588. doi:10.1172/JCI96061.

[38] Gordon SR, Maute RL, Dulken BW, Hutter G, George BM, McCracken MN, Gupta R, Tsai JM, Sinha R, and Corey D, et al (2017). PD-1 expression by tumour-associated macrophages inhibits phagocytosis and tumour immunity. *Nature* **545**(7655), 495–499. doi:10.1038/nature22396.

[39] Fang P, Li X, Dai J, Cole L, Camacho JA, Zhang Y, Ji Y, Wang J, Yang XF, and Wang H (2018). Immune cell subset differentiation and tissue inflammation. *J Hematol Oncol* **11**(1), 97. doi:10.1186/s13045-018-0637-x.

[40] Sallusto F, Lanzavecchia A, Mackay CR. Chemokines and chemokine receptors in T-cell priming and Th1/Th2-mediated responses. Immunology Today **1998**;19(12):568–74 doi https://doi.org/10.1016/S0167-5699(98)01346-2.

[41] De Palma M and Lewis CE (2013). Macrophage regulation of tumor responses to anticancer therapies. *Cancer Cell* **23**(3), 277–286. doi:10.1016/j.ccr.2013.02.013.

[42] Mazzieri R, Pucci F, Moi D, Zonari E, Ranghetti A, Berti A, Politi LS, Gentner B, Brown JL, and Naldini L, et al (2011). Targeting the ANG2/TIE2 axis inhibits tumor growth and metastasis by impairing angiogenesis and disabling rebounds of proangiogenic myeloid cells. *Cancer Cell* **19**(4), 512–526. doi:10.1016/j.ccr.2011.02.005.

[43] Harney AS, Karagiannis GS, Pignatelli J, Smith BD, Kadioglu E, Wise SC, Hood MM, Kaufman MD, Leary CB, and Lu WP, et al (2017). The Selective Tie2 Inhibitor Rebastinib Blocks Recruitment and Function of Tie2(Hi) Macrophages in Breast Cancer and Pancreatic Neuroendocrine Tumors. *Mol Cancer Ther* **16**(11), 2486–2501. doi:10.1158/1535-7163.MCT-17-0241.

[44] Coffelt SB, Chen YY, Muthana M, Welford AF, Tal AO, Scholz A, Plate KH, Reiss Y, Murdoch C, and De Palma M, et al (2011). Angiopoietin 2 Stimulates TIE2-Expressing Monocytes To Suppress T Cell Activation and To Promote Regulatory T Cell Expansion. *The Journal of Immunology* . doi:10.4049/jimmunol.1002802.

[45] Ibberson M, Bron S, Guex N, Faes-van't Hull E, Ifticene-Treboux A, Henry L, Lehr HA, Delaloye JF, Coukos G, and Xenarios I, et al (2013). TIE-2 and

VEGFR kinase activities drive immunosuppressive function of TIE-2-expressing monocytes in human breast tumors. *Clin Cancer Res* **19**(13), 3439–3449. doi:10.1158/1078-0432.Ccr-12-3181.

[46] Kalluri R (2016). The biology and function of fibroblasts in cancer. *Nat Rev Cancer* **16**(9), 582–598. doi:10.1038/nrc.2016.73.

[47] Lederle W, Hartenstein B, Meides A, Kunzelmann H, Werb Z, Angel P, and Mueller MM (2010). MMP13 as a stromal mediator in controlling persistent angiogenesis in skin carcinoma. *Carcinogenesis* **31**(7), 1175–1184. doi:10.1093/carcin/bgp248.

[48] Ozdemir BC, Pentcheva-Hoang T, Carstens JL, Zheng X, Wu CC, Simpson TR, Laklai H, Sugimoto H, Kahlert C, and Novitskiy SV, et al (2014). Depletion of carcinoma-associated fibroblasts and fibrosis induces immunosuppression and accelerates pancreas cancer with reduced survival. *Cancer Cell* **25**(6), 719–734. doi:10.1016/j.ccr.2014.04.005.